Pergamon

Int. J. Heat Mass Transfer. Vol. 37, No. 5, pp. 829–836, 1994

0017-9310/94 $6.00+0.00

Convective melting of packed beds

O. A. PLUMB

Department of Mechanical and Materials Engineering, Washington State University, Pullman, WA 99164-2920, U.S.A.

(*Received* 18 *December* 1992 *and in final form* 5 *August* 1993)

Abstract—The volume averaged equations for convective melting of particles in a packed bed are developed and a simple model is proposed. The model is solved numerically in one dimension to predict melting rates for a single substance and a system in which the liquid phase at elevated temperature enters a packed bed of the solid phase at the melting temperature. Materials having the thermophysical properties of water and aluminum are examined. For large Peclet number, the heat transfer is dominated by convection and the melting rate depends on the Stefan number, liquid to solid density ratio, fluid velocity and the initial solid fraction. The thickness of the melting zone increases with Peclet number and Prandtl number for systems dominated by convection.

INTRODUCTION

THE MELTING of solid particles in a liquid where a relative velocity between the liquid and fluid exists occurs in a large number of materials processing applications as well as in the environment. For example, solid materials are often poured into molten materials in smelting operations, alloying operations, and vitrification processes for both materials production and destruction of hazardous waste. In the environment an ice jam in a river is an example of melting of a packed bed of solids subject to a flowing liquid. In modelling severe nuclear accidents, engineers have also shown an interest in melting in packed beds. In some of these applications heavy solids are introduced to a molten liquid and melt as they settle. In others, the system behaves like a packed bed in that warmer liquid flows through a porous bed of solids at or near the melting temperature. The packed bed was selected for examination in this study because it offers the simpler alternative for examining some of the physics and is relatively easy to replicate experimentally.

In what follows the theory for melting in a packed bed will first be developed. This will involve starting with the liquid and solid phase energy equations and developing the two medium governing equations. The resulting model equations are solved numerically to demonstrate the effect of the key parameters on the melting process. Finally, the results are presented in a fashion that allows their use in engineering predictions for melting problems.

THEORETICAL FORMULATION

The theoretical formulation begins with the continuity and energy equations for the solid and liquid phases.

Continuity

$$\text{solid}: \quad \frac{\partial \rho_s}{\partial t} + \nabla \cdot (\rho_s v_s) = 0 \tag{1}$$

$$\text{liquid}: \quad \frac{\partial \rho_l}{\partial t} + \nabla \cdot (\rho_l v_l) = 0 \tag{2}$$

Energy

$$\text{solid}: \quad \frac{\partial}{\partial t}(\rho_s h_s) + \nabla \cdot (\rho_s h_s v_s) = -\nabla \cdot q_s \tag{3}$$

$$\text{liquid}: \quad \frac{\partial}{\partial t}(\rho_l h_l) + \nabla \cdot (\rho_l h_l v_l) = -\nabla \cdot q_l. \tag{4}$$

The appropriate interfacial conditions for conservation of mass and energy can be written as follows:

$$\rho_l (v_l - w) \cdot n_{l-s} + \rho_s (v_s - w) \cdot n_{s-l} = 0 \tag{5}$$

$$n_{l-s} \cdot k_l \nabla T_l + n_{s-l} \cdot k_s \nabla T_s = \rho_s (v_s - w) \cdot n_{s-l} h_s + \rho_l (v_l - w) \cdot n_{l-s} h_l \tag{6}$$

where w represents the velocity of the solid–liquid interface and the sign convention for the velocities and unit vectors is shown in Fig. 1.

The above system of equations could be solved numerically. However, the complexity of the geometry of the interface, A_{s-l}, where the interfacial boundary

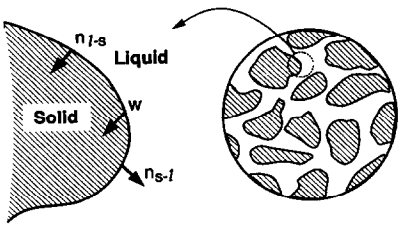

FIG. 1. The averaging volume and microscopic interface.

NOMENCLATURE

A	surface area per unit volume [m^{-1}]
c_p	specific heat at constant pressure [J kg^{-1} K^{-1}]
D^*	dimensionless diffusion coefficient defined in equation (40)
D_L	longitudinal dispersion coefficient [m^2 s^{-1}]
D_P	particle diameter [m]
h	convective heat transfer coefficient [W m^{-2} K^{-1}]
H	dimensionless parameter defined in equation (36)
k	thermal conductivity [W m^{-1} K^{-1}]
L	length scale defined as α_o/v_{l_o} [m]
$\dot{m}$	melting rate per unit volume [kg m^{-3} s^{-1}]
M	dimensionless melting rate defined in equation (37)
n	unit vector (see Fig. 1)
Nu	Nusselt number
Pe_{L_o}	Peclet number based on L and liquid inlet velocity
Pr	Prandtl number
q	heat flux [W m^{-2}]
R	ratio of liquid density to solid density
Re	Reynolds number based on particle diameter
S	dimensionless sink term in liquid phase energy equation defined in equation (41)
St	Stefan number defined in equation (43)
T	temperature [K]
t	time [s]
V	volume [m^3]
v	velocity [m s^{-1}]
w	velocity of the solid–liquid interface [m s^{-1}]
x	axial coordinate [m].

Greek symbols

α	thermal diffusivity [m^2 s^{-1}]
θ	dimensionless temperature defined in equation (32)
ρ	density [kg m^{-3}]
Φ	phase fraction
Ψ	a local property.

Subscripts

d	based on particle diameter
l	liquid phase
m	melting conditions
o	based on liquid inlet conditions
s	solid phase.

Superscript

*	indicates a dimensionless parameter.

conditions must be applied is for most practical problems sufficiently complex to render this alternative unfeasible. It is therefore desirable to simplify the problem by volume averaging over a region in the porous medium called a representative elementary volume or averaging volume as indicated in Fig. 1. In doing so liberal use will be made of the general transport theorem

$$\frac{\mathrm{d}}{\mathrm{d}t}\int_{V_\gamma}\psi\,\mathrm{d}V=\int_{V_\gamma}\frac{\partial\psi}{\partial t}\mathrm{d}V+\frac{1}{V}\int_{A}\psi w\cdot n\,\mathrm{d}A \tag{7}$$

the divergence theorem

$$\int_{V}\nabla\psi\,\mathrm{d}V=\int_{A}\psi n\cdot\mathrm{d}A \tag{8}$$

and the theorem for the volume average of a divergence [1]

$$\langle\nabla\cdot b\rangle=\nabla\cdot\langle b\rangle+\frac{1}{V}\int_{A}b\cdot n\,\mathrm{d}A \tag{9}$$

where the definition of a volume averaged quantity is written

$$\langle\psi\rangle=\frac{1}{V}\int_{V_\gamma}\psi\,\mathrm{d}V=\frac{\phi_\gamma}{V_\gamma}\int_{V_\gamma}\psi\,\mathrm{d}V. \tag{10}$$

Volume averaging the continuity equations and making use of the general transport theorem and the divergence theorem results in

$$\frac{\partial\langle\phi_s\rangle}{\partial t}+\nabla\cdot\langle v_s\rangle+\frac{1}{\rho_s V}\int_{A_{s-l}}\rho_s(v_s-w)\cdot n_{s-l}\,\mathrm{d}A=0 \tag{11}$$

$$\frac{\partial\langle\phi_l\rangle}{\partial t}+\nabla\cdot\langle v_l\rangle+\frac{1}{\rho_l V}\int_{A_{l-s}}\rho_l(v_l-w)\cdot n_{l-s}\,\mathrm{d}A=0 \tag{12}$$

where it has been assumed that both phases are incompressible. The integral terms in equations (11) and (12) when multiplied by the respective phase densities represent the mass flux across the interface and must be equal and opposite as expressed by the interfacial condition for mass (equation (5)). If we write

$$\dot{m}=-\frac{1}{V}\int_{A_{l-s}}\rho_l(v_l-w)\cdot n_{l-s}\,\mathrm{d}A=\frac{1}{V}\int_{A_{s-l}}\rho_s(v_s-w)\cdot n_{s-l}\,\mathrm{d}A \tag{13}$$

and assume $v_s=0$ then the continuity equations become

$$\frac{\partial\phi_l}{\partial t}+\nabla\cdot\langle v_l\rangle-\frac{\dot{m}}{\rho_l}=0 \tag{14}$$

$$\frac{\partial \phi_s}{\partial t} + \frac{\dot{m}}{\rho_s} = 0. \quad (15)$$

For the solid phase energy equation, again taking the solid phase velocity to be zero, volume averaging results in

$$\frac{\partial}{\partial t}\langle \rho_s h_s \rangle - \frac{1}{V}\int_{A_{s-l}} \rho_s h_s w \cdot n_{s-l}\, dA = \nabla \langle k_s \nabla T_s \rangle + \frac{1}{V}\int_{A_{s-l}} k_s \nabla T_s \cdot n_{s-l}\, dA. \quad (16)$$

Applying the averaging theorem a second time to the first term on the right hand side of equation (16) results in

$$\frac{\partial}{\partial t}\langle \rho_s h_s \rangle + \frac{1}{V}\int_{A_{s-l}} \rho_s h_s w \cdot n_{s-l}\, dA = \nabla \cdot [k_s \nabla \langle T_s \rangle] + \nabla \cdot \left[\frac{k_s}{V}\int_{A_{s-l}} T_s n_{s-l} \cdot dA\right] + \frac{1}{V}\int_{A_{s-l}} k_s \nabla T_s \cdot n_{s-l}\, dA. \quad (17)$$

Writing the enthalpy as the product of specific heat and temperature results in

$$\rho_s c_{p_s} \frac{\partial}{\partial t}\langle T_s \rangle - \frac{1}{V}\int_{A_{s-l}} \rho_s c_{p_s} T_{sw} \cdot n_{s-l}\, dA = \nabla \cdot [k_s \nabla \langle T_s \rangle] + \nabla \cdot \left[\frac{1}{V}\int_{A_{s-l}} T_s n_{s-l} \cdot dA\right] + \frac{1}{V}\int_{A_{s-l}} k_s \nabla T_s \cdot n_{s-l}\, dA \quad (18)$$

where the specific heat has been assumed to be constant.

The energy equation for the liquid phase is identical to that for the solid except that the liquid velocity is non-zero. Hence, we must deal with the convective term which can be volume averaged to obtain

$$\langle \rho_l c_{p_l} \nabla (T_l v_l) \rangle = \rho_l c_{p_l} \nabla \cdot \langle T_l v_l \rangle + \frac{1}{V_l}\int_{A_{l-s}} \rho_l c_{p_l} (T_l v_l) \cdot n_{l-s}\, dA. \quad (19)$$

Further simplification of the nonlinear term can result if Gray's decomposition [2] is applied by letting

$$T_l = \langle T_l \rangle^l + T_l' \quad \text{and} \quad v_l = \langle v_l \rangle^l + v_l'. \quad (20)$$

The first term on the right hand side of equation (19) can then be written

$$\rho_l c_{p_l} \nabla \cdot \langle T_l v_l \rangle = \rho_l c_{p_l} [\nabla \cdot (\langle T_l \rangle^l \langle v_l \rangle^l) + \nabla \cdot \langle T_l' v_l' \rangle]. \quad (21)$$

The second term in equation (21) represents the hydrodynamic dispersion. The energy equation for the liquid phase can now be written

$$\rho_l c_{p_l} \frac{\partial}{\partial t}(\phi_l \langle T_l \rangle^l) + \frac{1}{V_l}\int_{A_{l-s}} \rho_l (v_l - w) c_{p_l} T_l \cdot n_{s-l}\, dA + \rho_l c_{p_l} [\nabla \cdot (\phi_l \langle T_l \rangle^l \langle v_l \rangle)] + \rho c_{p_l} \nabla \cdot \langle T_l' v_l' \rangle = \nabla \cdot [\phi_l k_l \nabla \langle T_l \rangle^l] + \nabla \cdot \left[\frac{k_l}{V_l}\int_{A_{l-s}} T_l n_{l-s} \cdot dA\right] + \frac{1}{V}\int_{A_{l-s}} k_l \nabla T_l \cdot n_{l-s}\, dA. \quad (22)$$

The interfacial condition for energy can be obtained by integrating the interfacial condition expressed in equation (6) over the interfacial areas

$$\int_{A_{l-s}} n_{l-s} \cdot (k_l \nabla T_l - k_s \nabla T_s)\, dA = \int_{A_{l-s}} \rho_l (v_l - w)(h_l - h_s) \cdot n_{l-s}\, dA. \quad (23)$$

The system which includes equations (14), (15), (18), (22) and (23) still presents difficulties because of the integrals over surface areas. There exist at least two possible approaches to dealing with this difficulty. The first and most rigorous is to apply Gray's decomposition to all of the terms and to develop a closure theory for the small quantities [3]. The second approach is to build models for these terms which are based, as much as possible, on previous related experimental results. It is this latter approach which will be taken here in part because of expedience and in part because of the lack of experimental results for use in verifying a more rigorous theory.

MODEL FORMULATION

In order to simplify the theory developed in the previous section it will first be assumed that the solid phase is at the melting temperature. This is not an unreasonable approach for several of the applications mentioned in the Introduction. This results in the elimination of equation (18). In equation (22) the integral term on the left side of the equation represents an energy sink for sensible heat due to the melting solid entering the liquid phase at the melting temperature which is different from the liquid phase temperature. It can be modelled as

$$\frac{1}{V}\int_{A_{l-s}} \rho_l (v_l - w) c_{p_l} T_l \cdot n_{l-s}\, dA = -\dot{m} c_{p_l} T_m \quad (24)$$

where $\dot{m}$ is the rate of melting per unit volume and T_m is the melting temperture.

The last term on the left hand side of equation (22) is the dispersive transport. This term will be modelled through the inclusion of a dispersive contribution to the diffusion term in the model equation. The first integral term on the right hand side of equation (22) represents the effect of the interfacial geometry on

conduction through the liquid phase. This term is traditionally lumped into the first term on the right hand side of the equation by using an effective conductivity. This is a logical approach since it is the combination of both conduction terms that is measured experimentally to determine the effective conductivity for a fluid saturated porous medium.

The final integral term represents the heat transfer by conduction across the solid–liquid interface. This term can be modelled through the introduction of an empirical heat transfer coefficient

$$\frac{1}{V}\int_{A_{l-s}} \nabla T_l \cdot n_{l-s}\,dA = -hA_{l-s}(\langle T_l\rangle - T_m). \quad (25)$$

The energy interfacial condition (equation (23)) states that the latent heat required to melt the solid at the rate $\dot{m}$ must be equal to the heat conduction from the liquid to the solid phase when the solid phase is uniformly at the melting temperature, thus

$$\dot{m}h_{ls} = hA_{l-s}(\langle T_l\rangle - T_m). \quad (26)$$

The model system of equations can now be written

Solid phase continuity:

$$\frac{\partial \phi_s}{\partial t} + \frac{\dot{m}}{\rho_s} = 0 \quad (27)$$

Liquid phase continuity:

$$\frac{\partial \phi_l}{\partial t} + \frac{\partial}{\partial x}(\phi_l v_l) - \frac{\dot{m}}{\rho_l} = 0 \quad (28)$$

Liquid phase energy equation:

$$\frac{\partial(\phi_l T_l)}{\partial t} - \frac{\dot{m}T_m}{\rho_l} + \frac{\partial}{\partial x}(\phi_l T_l v_l) = \frac{\partial}{\partial x}\left[\left(\frac{k_{eff}}{\rho_l c_{p_l}} + D_L\right)\frac{\partial T_l}{\partial x}\right] - hA_{l-s}(T_l - T_m) \quad (29)$$

Energy jump condition:

$$\dot{m}h_{ls} = hA_{ls}(T_l - T_m) \quad (30)$$

where the brackets denoting volume averaged quantities have been dropped for the sake of simplicity. Making use of the liquid phase continuity equation results in a further simplification to the liquid phase energy equation

$$\frac{\partial T_l}{\partial t} + v_l\frac{\partial T_l}{\partial x} = \frac{\partial}{\partial x}\left[\left(\frac{k_{eff}}{\rho_l c_{p_l}} + D_L\right)\frac{\partial T_l}{\partial x}\right] - \left(\frac{hA_{l-s}}{\rho_l c_{p_l}\phi_l} + \dot{m}c_{p_l}\phi_l\right)(T_l - T_m). \quad (31)$$

The above model equations can be non-dimensionalized using the following scaling

$$t^* = \frac{t\alpha_o}{L^2}, \quad v_l^* = \frac{v_l}{v_{l_o}}, \quad x^* = \frac{x}{L}, \quad \theta = \frac{T_l - T_m}{T_{l_o} - T_m} \quad (32)$$

where α_o is the initial effective liquid phase diffusivity and v_{l_o} and T_{l_o} are the liquid velocity and temperature

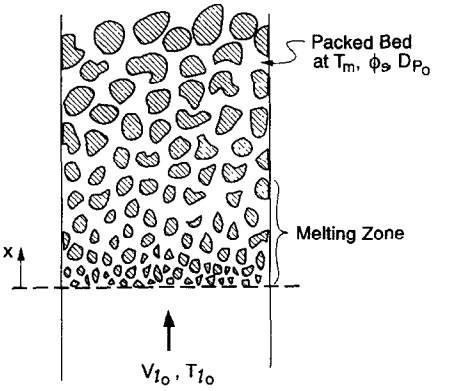

FIG. 2. One dimensional convective melting of a packed bed.

at the entrance to the packed bed as illustrated in Fig. 2. The characteristic length L can be selected in a variety of ways depending on whether the problem is convection or diffusion dominated. For the sake of this study L has been selected to be α_o/v_{l_o} resulting in fixing the scaled Peclet number at unity. The dimensionless model equations can now be written

$$\frac{\partial \phi_s}{\partial t^*} + M = 0 \quad (33)$$

$$\frac{\partial \phi_l}{\partial t^*} + Pe_{L_o}\frac{\partial v_l^*}{\partial x^*} - \frac{M}{R} = 0 \quad (34)$$

$$\frac{\partial \theta}{\partial t^*} + Pe_{L_o}v_l^*\frac{\partial \theta}{\partial x^*} = \frac{\partial}{\partial x}\left(D^*\frac{\partial \theta}{\partial x}\right) - S\theta \quad (35)$$

$$M = H \cdot R \cdot St \cdot \theta. \quad (36)$$

The parameters appearing in the above set of equations are defined as follows:

$$M = \frac{L^2\dot{m}}{\alpha_o\rho_s} \quad (37)$$

$$Pe_{L_o} = \frac{v_{l_o}L}{\alpha_o} \quad (38)$$

$$R = \frac{\rho_l}{\rho_s} \quad (39)$$

$$D^* = \left(\frac{\alpha_{eff} + D_L}{\alpha_o}\right) \quad (40)$$

$$S = \frac{L^2(hA_{ls} + \dot{m}c_{p_l})}{\alpha_o\phi_l\rho_l c_{p_l}} \quad (41)$$

$$H = \frac{L^2hA_{ls}}{k_{eff_o}} \quad (42)$$

$$St = \frac{c_{p_l}(T_{l_o} - T_m)}{h_{ls}}. \quad (43)$$

The boundary and initial conditions applied in this study are

$$\theta = 1, \quad \phi_l = \phi_{l_o}, \quad \phi_s = \phi_{s_o} \quad \text{at } t^* = 0$$

$$v_l^* = 1, \quad \theta = 1 \quad \text{at } x^* = 0$$

$$\theta = 0 \quad \text{at } x^* \to \infty. \tag{44}$$

Before the system consisting of equations (33)–(36) and (44) can be solved the transport properties h, k_{eff}, and D_L, must be defined and a model which couples the surface area per unit volume, A_{ls}, to the porosity or melting rate must be developed.

The effective thermal conductivity will be modelled using the geometric mean which is in good agreement with the available experimental data for $k_s/k_l < 10$ [4]

$$k_{\text{eff}} = k_l^{\phi_l} k_s^{\phi_s}. \tag{45}$$

Following the recommendation of Wakao and Kaguei [5] the dispersion coefficient and the convective heat transfer coefficient are computed from

$$\frac{D_L}{\alpha_l} = 0.5\, Pe_{D_P} \tag{46}$$

$$Nu_{D_P} = 2 + 1.1 Re_{D_P}^{0.6} Pr^{1/3} \tag{47}$$

where the Peclet and Reynolds numbers are based on the particle diameter and the properties are liquid properties.

Equations (46) and (47) add the requirement that the particle diameter D_P be known as part of the required relationship between surface area and porosity or melting rate. The end result is a 'geometric' melting model. There are two possible simple models which could be developed. The first is a constant porosity model. In this case the particles making up the packed bed would be assumed to retain their sphericity as they melt and constantly repack resulting in a changing volume for the bed. In this case the porosity would remain constant. It is noted that for this model the permeability, which is proportional to particle diameter squared, would approach zero as the particles melt, eventually resulting in a plugged bed. This coupled with the repacking requirement leads one to believe that a constant porosity model may be unrealistic.

The second possible melting model is a constant volume model. In this case the porosity increases during melting, however, the total volume remains constant except at the entrance where the solid is completely melted. If one forces the particles to remain spherical then the bed is no longer 'packed' once melting begins. Thus, this model is unrealistic unless the melting is assumed to be nonuniform on the individual spheres resulting in a geometry like that sketched in Fig. 3. In this case the precise applicability of equations (46) and (47) could be questioned. In all likelihood, the actual melting geometry might be somewhere in between the constant volume and the constant porosity models. In this paper the constant volume model will be pursued because, at least from the intuitive standpoint, it seems to be the most realistic.

In order to compute the surface area per unit volume the initial packing of the bed will be assumed to be body centered cubic resulting in

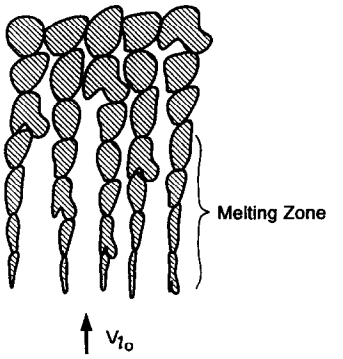

FIG. 3. Sketch of the microscopic geometry consistent with the constant volume melting model.

$$A_{ls} = \frac{16\pi}{\left(\sqrt{\frac{16}{3}}\right)^3 D_P} \quad \text{and} \quad \phi_s = 0.68. \tag{48}$$

Despite the fact that the particles cannot remain spherical in a constant volume process it will be assumed that the relationship given by equation (48) between surface area and 'effective' particle diameter continues to be applicable during melting.

Effective particle diameter can be related to the melting rate again through the assumption of body centered cubic packing since the number of particles per unit volume is given by

$$N = \frac{2}{\left(\sqrt{\frac{4}{3}}\right)^3 D_P^3}. \tag{49}$$

The relationship between the particle size and the dimensionless melting rate can now be written

$$\frac{dD_P^3}{dt^*} = -3\sqrt{(4/3)^3}\, M D_P^3. \tag{50}$$

This result is utilized to predict the local effective particle diameter which in turn is used in predicting the local dispersion coefficient and convective heat transfer coefficient as given by equations (46) and (47).

The model developed above has been solved numerically using an implicit method. The equations were discretized using the power law differencing scheme as described by Raithby and Schneider [6]. Calculations were completed for two materials having vastly different properties—one having the properties of water and another having the properties of aluminum. The thermophysical properties utilized in the calculations are listed in Table 1.

The grid size and time step necessary to achieve satisfactory results were dependent on the magnitude of the particle Reynolds number. For each case several numerical calculations were completed while successively decreasing the grid size and time step. It was judged that the grid size and time step were sufficiently small when the thickness of the melt zone became

Table 1. Thermophysical properties

	ρ_l [kg m^{-3}]	ρ_s [kg m^{-3}]	μ_l [N s m^{-2}]	Pr	k_l [W m^{-1} K^{-1}]	k_s [W m^{-1} K^{-1}]	c_{pl} [J kg^{-1} K^{-1}]	h_{sl} [kJ kg^{-1}]
Water	1000	920	1422×10^{-6}	10	0.57	1.9	4180	333
Aluminum	2370	2700	2.8×10^{-3}	0.03	104	213	1084	400

independent of these two parameters. The melt zone is defined as the region over which the solid fraction varied from zero to the initial solid fraction of 0.68.

DISCUSSION OF RESULTS

All of the results presented are for an initial particle diameter of 1 mm. Aside from the different thermophysical properties, the effect of the inlet velocity or particle Reynolds number and the Stefan number were examined. Typical results for water ($Pr = 10$) with a Stefan number of 0.1, and a particle Reynolds number of 0.1 are shown in Fig. 4. For this case the heat transfer in the flow direction is dominated by diffusion as opposed to convection. The figure presents dimensionless temperature and solid fraction as a function of distance into the bed for several times. Real time and dimensional distance are shown instead of dimensionless quantities for comparative purposes. The results show that in a matter of a few seconds the melting front begins to propagate through the packed bed. After an initial transient period the model indicates a constant propagation velocity. In this case the melting front is propagating at approximately 1.3×10^{-4} m s^{-1}.

Results for one order of magnitude increase in velocity are shown in Fig. 5 for the same properties. In this case the front begins to propagate into the bed in less than 15 s. The effect of the increase in convective transport of heat into the bed as opposed to diffusive transport can be seen in the thicker melting zone. That is, the region over which the solid fraction changes from zero to the initial solid fraction ($\phi_{sl} = 0.68$) is wider. The same trend is observed when the velocity is increased by another order of magnitude as illustrated in Fig. 6 for the case of a particle Reynolds number (based on the inlet velocity) of 10.

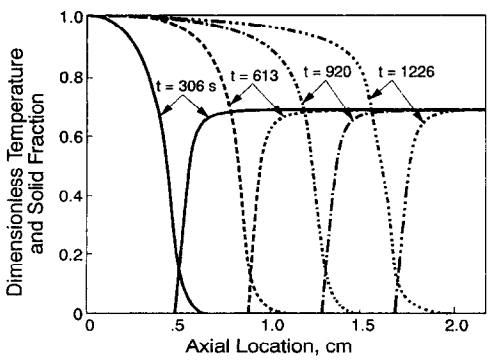

FIG. 4. Dimensionless temperature and solid fraction in the melting zone (water, $Re = 0.10$, $Ste = 0.10$).

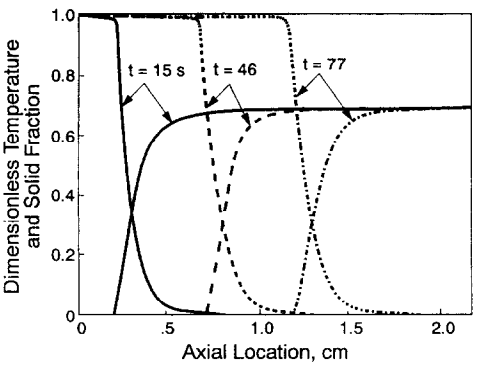

FIG. 5. Dimensionless temperature and solid fraction in the melting zone (water, $Re = 1$, $Ste = 0.10$).

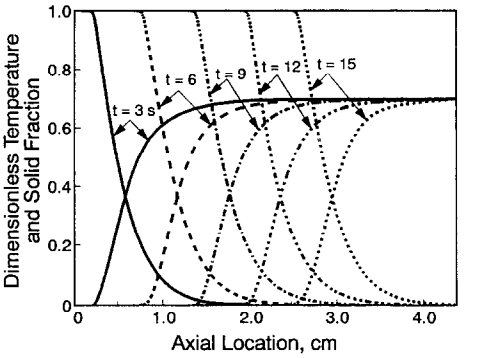

FIG. 6. Dimensionless temperature and solid fraction in the melting zone (water, $Re = 10$, $Ste = 0.10$).

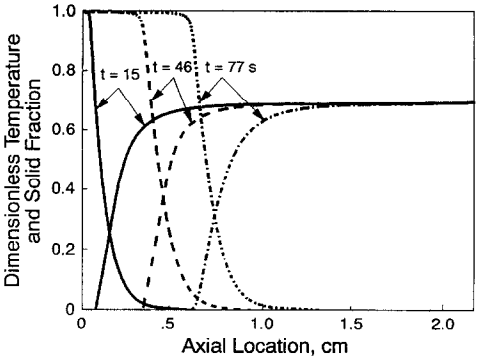

FIG. 7. Dimensionless temperature and solid fraction in the melting zone (water, $Re = 1$, $Ste = 0.05$).

The temperature distribution in the melt zone shows little effect of axial thermal dispersion, even at higher particle Reynolds number because of the small axial length scale associated with the melt zone.

The effect of reducing the Stefan number by a factor of 2 to 0.05 is illustrated in Fig. 7 for a case otherwise

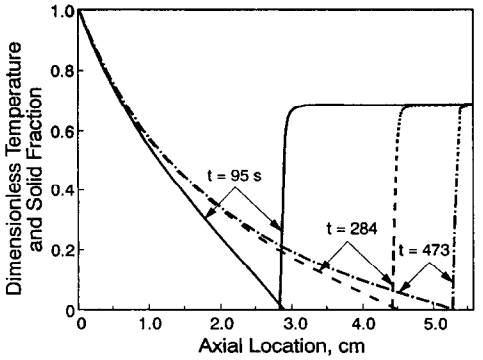

FIG. 8. Dimensionless temperature and solid fraction in the melting zone (aluminum, $Re = 1$, $Ste = 0.15$).

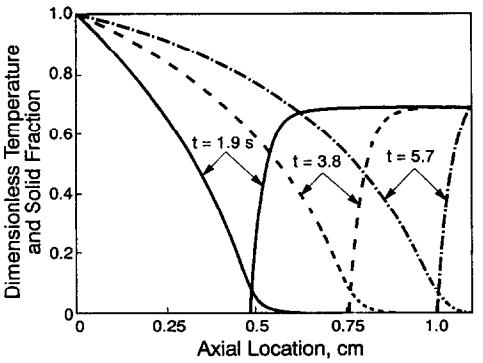

FIG. 9. Dimensionless temperature and solid fraction in the melting zone (aluminum, $Re = 10$, $Ste = 0.15$).

identical to the case shown in Fig. 5 (an inlet particle Reynolds number of 1.0). The two sets of results are nearly identical except for the melting process being slowed by a factor of two since the melting rate is linearly dependent upon the Stefan number as might be expected for small Stefan number.

Results for a low Prandtl number material having properties similar to aluminum are shown in Figs. 8–10. In this case the Stefan number is 0.15 and the Prandtl number is 0.03. Figure 8 illustrates that the process is strongly conduction dominated for the case of an inlet velocity that results in a particle Reynolds number of 1.0. The temperature distribution is nearly linear, however, the melting zone is the same order of magnitude as that for the high Prandtl number case (water). As the inlet velocity is increased the increased dominance of the effects of convection can be seen in Figs. 9 and 10. In Fig. 9, for a particle Reynolds number of 10, there is still some conduction to the upstream boundary whereas in Fig. 10 ($Re_P = 100$) the heat transfer becomes dominated by convection and a nearly constant melt propagation velocity of 1.36×10^{-2} m s^{-1} results. The effect of Stefan number is the same as that observed for water in that a decrease by a factor of two results in a similar decrease in the melting rate.

The quantity of primary interest from the practical standpoint is the melting rate under steady state conditions. Under steady conditions a front propagation velocity can be estimated using global energy and mass balances on the melting zone. The end result is that the melting zone will propagate at a velocity given by

$$v_{\text{Front}} = \frac{R\,Ste\,v_{\text{lo}}}{\phi_s + R\,Ste}. \tag{51}$$

This result can be utilized to check the numerical results. However, it must be noted that equation (51) does not account for heat transfer by conduction upstream of the melt zone. Thus, the comparison between equation (51) and the numerical results must be expected to be better for water than for aluminum because of the much lower thermal conductivity of water. The comparison should also be better under conditions where convection is dominant. Comparison between the theoretical and experimental propagation velocities is shown in Fig. 11 as a function of particle Reynolds number.

The melt zone thickness will increase as the liquid velocity is increased. Figure 12 shows the melt zone thickness as a function of particle Peclet number. These results are independent of the Stefan number but depend on the Prandtl number. Higher Prandtl numbers lead to a thicker melt zone. As the heat transfer becomes diffusion dominated at low Peclet number the zone thickness becomes independent of

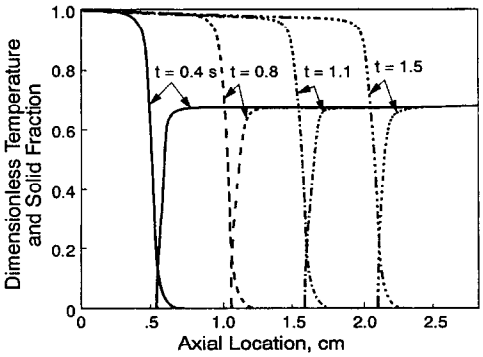

FIG. 10. Dimensionless temperature and solid fraction in the melting zone (aluminum, $Re = 100$, $Ste = 0.15$).

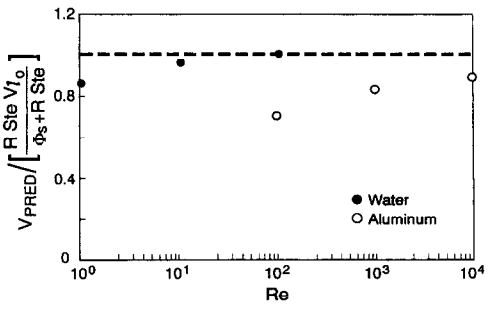

FIG. 11. Predicted and steady state melt zone propagation velocity as a function of particle Reynolds number.

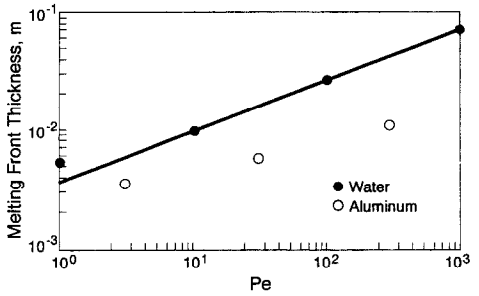

FIG. 12. Melting zone thickness (dimensional) as a function of particle Peclet number.

the Peclet number. In the convection dominated regime ($Pe \geqslant 10$) the melt zone thickness increases with the Peclet number to a power slightly greater than 0.4 for water.

CONCLUSIONS

The volume averaged equations for melting of a packed bed have been developed. These equations are modelled to predict melting rates for a single substance which are applicable to either the case of liquid entering a stagnant packed bed or a cloud of particles falling (or rising in the case of ice and water) through a stagnant liquid.

The results demonstrate that for systems dominated by convection (large Peclet number based on particle diameter) the velocity of the melting front can be predicted using a simple steady state solution. In this case the front propagation velocity depends only on the Stefan number, the liquid/solid density ratio, the fluid velocity and the solid fraction. For low Peclet numbers the front propagation rate falls below the steady state solution.

The thickness of the melting zone increases as a power law of the Peclet number and is independent of the Stefan number for systems which are dominated by convection. The melt zone thickness is greater for larger Prandtl numbers.

Acknowledgements—This material is based upon work supported by the National Science Foundation under Grant No. CTS-9016104. The author would like to express his appreciation to an anonymous reviewer who pointed out an error in the theoretical formulation.

REFERENCES

1. S. Whitaker, A simple geometrical derivation of the spatial averaging theorem, *Chem. Engng Ed.* **19**, 18–21 and 50–52 (1985).
2. W. G. Gray, A derivation of the equations for multiphase transport, *Chem. Engng Sci.* **30**, 229–233 (1975).
3. G. H. Crapiste, E. Rotstein and S. Whitaker, A general closure scheme for the method of volume averaging, *Chem. Engng Sci.* **41**, 227–235 (1986).
4. M. Kaviany, *Principles of Heat Transfer in Porous Media*, Chap. 3. Springer, New York (1991).
5. N. Wakao and S. Kaguei, *Heat and Mass Transfer in Packed Beds*. Gordon and Breach, New York (1982).
6. W. J. Minkowycz, E. M. Sparrow, B. E. Schneider and R. H. Pletcher, *Handbook of Numerical Heat Transfer*, Chap. 7. Wiley, New York (1988).